THE JOURNAL OF PHYSICAL CHEMISTRY A

pubs.acs.org/JPCA Article

Probing Surface Photovoltage Effect Using Photoassisted Secondary Electron Emission

Published as part of The Journal of Physical Chemistry virtual special issue "Time-Resolved Microscopy".

Yu Li, Usama Choudhry, Jeewan Ranasinghe, Alex Ackerman, and Bolin Liao*

Cite This: https://dx.doi.org/10.1021/acs.jpca.0c02543 Read Online

ACCESS | Metrics & More | Article Recommendations

ABSTRACT: While the properties of surfaces and interfaces are crucial to modern devices, they are commonly difficult to explore since the signal from the bulk often masks the surface contribution. Here we introduce a methodology based on scanning electron microscopy (SEM) coupled with a pulsed laser source, which offers the capability to sense the topmost layer of materials, to study the surface photovoltage (SPV) related effects. This method relies on a pulsed optical laser to transiently induce an SPV and a continuous primary electron beam to produce secondary electron (SE) emission and monitor the change of the SE yield under laser illumination. We observe contrasting behaviors of the SPV-induced SE yield change on n-type and p-type semiconductors. We further study the dependence of the SPV-induced SE yield on the primary electron beam energy, the optical fluence, and the modulation frequency of the optical excitation, which reveal the details of the dynamics of the photocarriers in the presence of the surface built-in potential. This fast, contactless, and bias-free technique offers a convenient and robust platform to probe surface electronic phenomena, with great promise to probe nanoscale effects with a high spatial resolution. Our result further provides a basis to understand the contrast mechanisms of emerging time-resolved electron microscopic techniques, such as the scanning ultrafast electron microscopy.

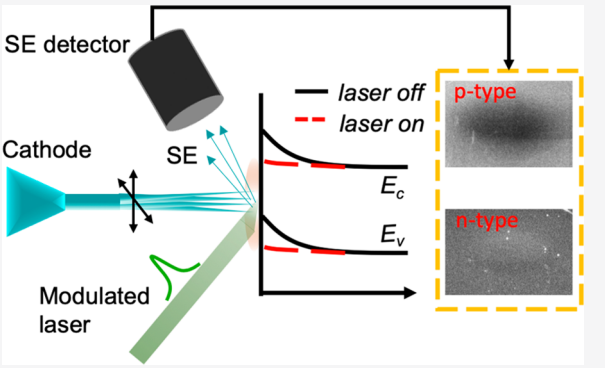

INTRODUCTION

Surfaces and interfaces are of paramount importance to semiconductors as they manipulate charge carrier dynamics and are fundamental to energy losses.[1−3] In addition, modern devices are being more investigated and produced in terms of their nanoscale morphologies/structures, which facilitate the exposure of surfaces substantially. While the periodic structure of an ideal crystalline semiconductor results in the forbidden band gaps, the termination of crystal structures at the free surface could generate energetical surface states within the band gaps.[2] Commonly, majority charge carriers are trapped at the surface states, followed by a net charge redistribution within a thin space-charge region (SCR). As a result, a built-in electric field is formed in the SCR while the bulk remains quasi-neutral. Upon superband photoillumination, photogenerated electron−hole pairs are separated by the built-in field and drift toward opposite directions. Specifically, the minority carriers are driven toward the surface to neutralize the surface majority charge, thus reducing the surface built-in potential. This change of surface potential caused by photoillumination is termed the surface photovoltage (SPV) effect,[4] which is of paramount importance regarding the working mechanism of semiconducting devices.[5−7] Therefore, many efforts have been focused on the detection, understanding, and manipulation of the SPV effect.[7−13]

A common way to detect the SPV effect is via the Kelvin probe measurement, in which a probe tip approaches the sample surface to generate a contact potential difference (CPD).[11] The difference between the values of CPD in dark and under illumination represents the SPV. However, the Kelvin probe measurement is usually time-consuming and can induce other effects by applying a voltage on the tip, such as ion migration,[14] masking the contribution from electronic surface states. A related method, SPV spectroscopy (SPS), is a well-established experimental technique to detect illumination-induced changes in the surface voltage.[4] However, it employs a semitransparent electrode deposited on top of the sample surface as the probe, which requires extra fabrication steps and

Received: March 23, 2020
Revised: June 2, 2020
Published: June 3, 2020

inevitably changes the surface condition.[15] The SPV effect has also been studied using scanning tunneling microscopy (STM), which requires a scanning probe as well.[9] In this light, a fast, contactless, and bias-free measurement would be desirable.

A promising candidate for this purpose is the scanning electron microscope (SEM), which can realize rapid and contactless measurements of the SPV with high spatial resolution and sufficient sensitivity when coupled with a light source.[16] While SEM is most widely used for imaging the sample topography, it is capable of detecting contrast in secondary electron (SE) emissions induced by other mechanisms. One of the attractive applications of low-voltage SEMs is to image the contrast between differently doped semiconductors regions, which was first observed in 1967 that the SE yield changes across a p−n junction.[17] It is well established that the SE yield is enhanced (suppressed) in the p-type (n-type) region, which looks brighter (darker) than the undoped region in an SEM. However, this method using SEM was only minimally reported until the 1990s thanks to the large improvements in electron sources, optics and detectors. In 1995, Perovic et al. observed SEM contrasts in p−n superlattices of silicon and GaAs and attributed the doping layer contrast to the surface-induced band bending differences between n- and p-doped layers.[18] Facilitated by this work, a series of investigations have been performed and the low-voltage SEM mode has been demonstrated to have a high sensitivity over a wide range of doping concentrations (10^{15}–10^{22} cm^{-3}).[16,19] It is generally accepted that the SE contrast of different doping types and concentrations in low-energy SEMs originates from the surface band bending effect in doped semiconductors, where the surface built-in potential helps (impedes) the SE escape in p-type (n-type) semiconductors. In comparison, other contributions such as atomic number differences related with backscattered electrons become dominant in higher electron voltage modes (i.e., >5 keV). Consequently, SEM should be able to characterize the SPV effect by quantifying the changed SE emission with superband illumination with low electron beam energies. Najafi et al. has used scanning ultrafast electron microscope (SUEM) to study the SPV effect in doped silicon.[7] However, a high-energy (30 keV) electron beam was used in their experiment, where the SE yield is much lower than for the lower-energy electron beams.[20]

In this work, we demonstrate the capability of detecting SPV in doped silicon by combining a conventional SEM with a pulsed laser beam. The laser beam is focused onto the sample surface and induces the SPV effect, which manifests itself in the contrast change of the SEM SE images. By modulating the laser beam using an acousto-optical modulator (AOM) and measuring the SE yield signal with a lock-in amplifier (LIA), we can record the amplitude and phase responses, which carry the information on the SPV effect, in a straightforward and steady-state manner. Specifically, the laser illumination induces a reduction (enhancement) in the SE signal for downward (upward) band bending, corresponding to p-type and n-type semiconductors, respectively.[2] As a result, the doping type of a semiconductor sample can be determined by the phase information. The change of the signal amplitude as a function of the illumination intensity is an indicator of the extent of the surface band bending compensation by photogenerated carriers. Furthermore, the dependence of the amplitude and the phase signal on the AOM modulation frequency can reveal the time scale of the underlying surface charge transfer processes. Our development of this photoassisted SE emission technique provides a novel strategy to derive information about the SPV effect and other mechanisms that contribute to the SE emission. We note that Flesner and O'Brien demonstrated a primitive setup with a similar concept[21] in 1989 to image the SPV effect in semiconductors. However, no quantitative analysis on the amplitude and the temporal information on the SPV effect was available in their work due to instrument limitations on the measurement sensitivity at the time.

EXPERIMENTAL SECTION

Figure 1a illustrates schematically our experimental apparatus for the SPV detection. The sample is mounted on a standard

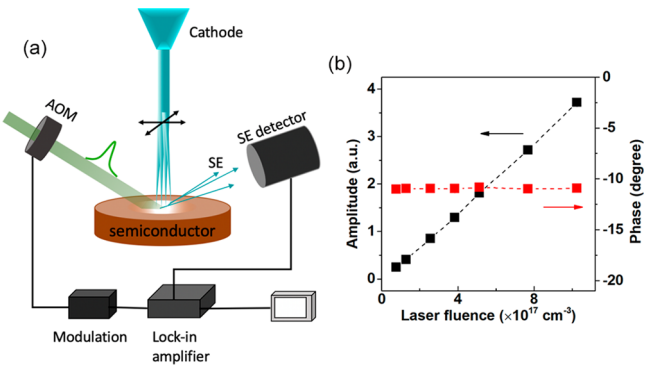

Figure 1. (a) Schematic of the experimental setup. (b) Amplitude and the phase signal of the laser leakage into the SE detector measured at 20 kHz modulation frequency.

SEM stage with a working distance of 10 mm from the pole piece. Optics are mounted outside a transparent window on the SEM chamber to allow a frequency-doubled green laser beam (515 nm) from a pulsed fiber laser (Clark-MXR, IMPULSE, 1030 nm, pulse duration 250 fs, repetition rate 5 MHz) to come through as the pump with an incident angle of ~40°. The laser beam size is about 100 μm. We calculate that ~30% of the incident light is reflected from the Si sample surface. The laser fluence (in the unit of photon number per volume) is calculated using the absorbed optical pulse energy divided by the absorption volume (the laser beam area times the optical absorption depth). Before entering the chamber, the laser beam is modulated by an acousto-optic modulator (AOM) with varying modulation frequencies from 2 kHz to 200 kHz.

Continuous primary electron beams with a beam current of ~130 pA, measured with a picoammeter and a Faraday cup, and different kinetic energies (2, 5 and 10 keV) are used to impact the sample surface and generate SEs. The SEs emitted from the sample surface are collected by a standard Everhart−Thornley detector (ETD), whose signal is delivered to a LIA via a BNC cable. The LIA reads out the component of the ETD signal at the modulation frequency of the AOM. The pump modulation and lock-in detection scheme not only significantly increases the signal-noise ratio of the measurement but also provides additional information on the time constants of the SPV response. During measurements, the output was collected by raster-scanning a small area near the center of the laser irradiated region with a magnification of 10 000 and an electron beam dwell time of 1 μs. These

https://dx.doi.org/10.1021/acs.jpca.0c02543
J. Phys. Chem. A XXXX, XXX, XXX−XXX

measurement parameters were chosen to minimize the beam damage of the sample surface and beam-induced contaminant deposition while maintaining an acceptable signal-to-noise ratio. Before and after each measurement, we checked that the SE yield from the beam-impacted location did not change appreciably.

The goal of the measurement is to quantify how the SE yield changes when the sample surface is under optical illumination, and how the SE yield change is affected by other parameters, including the electron beam kinetic energy, the optical fluence and the AOM modulation frequency. Since the standard ETD is not designed to be light-tight, some of the laser light inside the SEM chamber can leak through the ETD and generate an artificial signal not related to the sample response. To mitigate this effect, optical filters are inserted inside the ETD to minimize the leakage of the 515 nm pump light. With the optical filters in place, only a low level of pump light leakage can be detected, as shown in Figure 1b. This leakage signal is measured by reading the ETD when the optical pump is present inside the SEM chamber and the electron beam is turned off. In subsequent measurements, the light leakage signal is subtracted from the total signal measured by the ETD, and the remaining part represents the response from the sample. Although the light leakage signal is an artifact of the experimental setup, it can be useful as a reference for the phase signal and its dependence on the AOM modulation frequency indicates the intrinsic response time of the instrument.

A number of doped and undoped Si samples (MTI Corp.) are investigated. A general cleaning procedure (ultrasonic cleaning with acetone, IPA and deionized water for 5 min, respectively) with or without a subsequent hydrofluoric acid dip to remove the surface oxides were used to clean the samples before putting them in the SEM chamber. No appreciable difference beyond statistical uncertainty was observed between the two approaches, implying that our measurements with primary electron energies above 2 keV were not strongly affected by the surface oxide layer. Doping concentrations of the n-type and the p-type Si samples are estimated to be in the range of 10^{19} cm^{-3} on the basis of the electrical resistivity data.

RESULTS AND DISCUSSION

1. SPV Contrast on n-Type and p-Type Si. A schematic of the SPV effect on the surface of n-type and p-type Si is shown in Figure 2a. Without photoexcitation, the bulk electronic states and the surface states are in thermal equilibrium. Due to the charge transport between the bulk and the surface states, a space charge region is formed near the surface, within which majority carriers are depleted. The thickness D of the space charge region is given by

$$D = \frac{\rho_s}{N_d} \tag{1}$$

where ρ_s is the surface states density and N_d is the bulk doping concentration. Within the space charge region, the surface band bends upward (downward) in n-type (p-type) Si. The amount of surface band bending; i.e., the surface potential, V_s, is related to the surface states density, ρ_s, through the equation[2]

$$|V_s| = \frac{e\rho_s^2}{2\varepsilon_r\varepsilon_0 N_d} \tag{2}$$

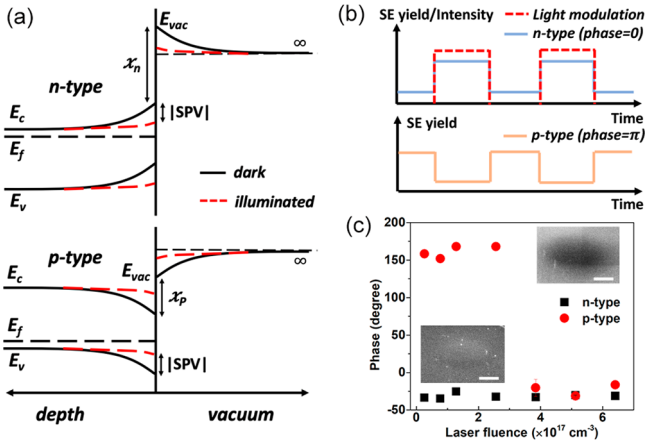

Figure 2. (a) Schematic showing the surface band bending and the SPV effect in n-type and p-type silicon. The thermal equilibrium between the bulk and the surface states can lead to a significant band bending in doped semiconductors. Upon photoexcitation of these samples, the surface states can be compensated by minority carriers, reducing the surface band bending and resulting in changes in the surface potential (the SPV effect). E_c: the conduction band bottom. E_v: the valence band top. E_f: the Fermi level. E_{vac}: the vacuum level. $\chi_{n,p}$: the electron affinity. (b) Illustration of the lock-in phase output, which is determined by the variation of the SE yield with respect to the laser modulation. (c) Phase signal as a function of the laser fluence for n-type and p-type Si with a modulation frequency of 50 kHz and an electron beam energy 2 keV. The insets include a SEM image of the n-type Si when the optical excitation is present and another image for the p-type Si, showing the bright and dark contrasts due to the SPV, respectively. The SEM images were taken at 2 keV with a fluence of 1×10^{17} cm^{-3}. The scale bars are 50 μm. Phase reversal occurs for p-type Si when the laser fluence is above 3.5×10^{17} cm^{-3}.

where e is the electron charge, ε_r is the relative permittivity of the material, and ε_0 is the vacuum permittivity. V_s is positive in p-type silicon and negative in n-type silicon.

The surface band bending leads to a built-in surface electric field that impacts the transport of the SEs. In n-type silicon, the built-in electric field points from inside the material toward the surface, thus impeding the transport of the SEs toward the sample surface. In p-type silicon, the built-in electric field points to the opposite direction and thus facilitate the SE transport process. This effect of the surface built-in electric fields is the underlying reason for the brighter (darker) SEM images of p-type (n-type) semiconductors compared to results for undoped semiconductors.[18,22−24] The one-dimensional constant-energy-loss model for the SE yield δ (number of SEs emitted per incident primary electron with energy E_{PE}) is given by[25]

$$\delta = B\frac{E_{PE}}{\xi}\frac{\lambda}{R}(1 - e^{-R/\lambda}) \tag{3}$$

where R is the total penetration depth of the primary electrons, λ is the SE escape length, B is the escape probability of an SE once it migrates to the sample surface, and ξ is the average energy cost to excite one SE. The SE escape length λ was previously estimated to be 2.7 nm in undoped Si.[20] The total penetration depth R of the primary electrons scales with the primary electron energy E_{PE} in a power law $R \propto E_{PE}^n$, where n is a constant ranging from 1.35 to 1.66.[25] R has been measured in Si to be 120 nm when E_{PE} = 2 keV, which increases to 350 nm

https://dx.doi.org/10.1021/acs.jpca.0c02543
J. Phys. Chem. A XXXX, XXX, XXX−XXX

when E_{PE} = 5 keV.[26] In this study, $R \gg \lambda$ is valid for all primary electron energies we use, so eq 3 can be simplified to

$$\delta \propto \frac{B}{\xi}\frac{\lambda}{{E_{PE}}^{n-1}} \tag{4}$$

Both the SE escape probability B and the SE escape length λ are affected by the surface electric field. B is largely determined by the electron affinity $X_{n,p}$ at the surface (Figure 2a), which is not directly changed by the surface electric fields. The dominant effect[24] is the exponential dependence of λ on the surface electric field,[27] in particular when the SE escape length is smaller than the thickness of the space charge region (in a later section, we estimate the space charge region thickness in our samples is around 10 nm):

$$\lambda(V_s) = \lambda(0)e^{V_s/(DF)} \tag{5}$$

where $\lambda(0)$ is the SE escape length when there is no surface band bending and F is a constant electric field, typically on the order of the breakdown electric field in Si (6×10^5 V/cm).[24] The sign of V_s determines whether the SE escape length is increased (p-type) or decreased (n-type).

When the doped semiconductors are under optical illumination, photogenerated electron−hole pairs are separated by the surface electric field. Minority carriers will be driven toward the surface and neutralize the surface majority charge that occupies the surface states. This process reduces the surface band bending and the built-in electric fields, leading to a change of the surface potential, which is the origin of the SPV effect. As a leading-order approximation, we assume that the photogenerated minority carriers are all driven to the surface and thus reduce the surface charge density; i.e., the surface charge density ρ_s is modified to

$$\rho_s = \rho_{s,0} - I_{ph}\eta \tag{6}$$

where $\rho_{s,0}$ is the surface charge density without illumination, I_{ph} is the absorbed optical fluence, and η is the optical absorption depth. Combining eqs 2 and 6, we can see that the optical illumination suppresses the surface potential V_s, and the change of the surface potential V_s is the SPV (Figure 2a). Furthermore, combining eqs 2, 5, and 6, we see that the SPV induces a change in the SE yield:

$$\delta(I_{ph}) \propto \frac{B}{\xi}\frac{\lambda(0)}{{E_{PE}}^{n-1}}\exp\left[\pm\frac{e(\rho_{s,0} - I_{ph}\eta)^2}{2\varepsilon_r\varepsilon_0 N_d DF}\right] \tag{7}$$

where the positive (negative) sign corresponds to p-type (n-type) silicon. The difference between the secondary electron yields under illumination $\delta(I_{ph})$ and without illumination $\delta(0)$ generates the contrasts seen in the SEM images. In n-type silicon, the suppression of the surface band bending facilitates SE transport toward the surface and thus increases the SE yield. So a bright contrast on n-type silicon is expected within the laser illumination region as compared to the region without the laser illumination. The opposite effect (dark contrast) should be expected on p-type silicon.

These effects are observed in our experiment, as Figure 2c shows the bright (dark) SE contrast within the optical illumination area on n-type (p-type) Si samples. These observations indicate that the semiconductor type can be determined by tracking the differences between SE signals in dark and under illumination conditions. The phase information on the SE signals is also a handy indicator for this purpose.[10,15] Confirmed from the SE images, SE signal should increase (decrease) for the upward (downward) band bending under illumination. Consider the ideal case of rapid carrier generation, redistribution, and recombination processes, which do not introduce any phase retardation of the SE signal with respect to the AOM modulation of the optical pump, the phase would be 0 for upward band bending and π for downward band bending cases (Figure 2b). For the real case, due to the phase retardation from the light-induced dynamic processes, the phase is in the fourth quadrant and second quadrant for the upward (n-type) and downward (p-type) band bending scenarios, respectively. For example, Figure 2c shows the phase of the SE signal with a modulation frequency of 50 kHz for doped Si samples, which was −31° and +152° for the n-type and p-type, respectively, in line with the aforementioned physical picture. Interestingly, a phase reversal occurs in p-type Si when the laser fluence is above 3.5×10^{17} cm^{-3}. This is related to the full compensation of the surface states by photogenerated minority carriers, i.e., when $\rho_{s,0} = I_{ph}\eta$. Beyond this optical fluence, the surface electronic bands are flat and no longer affect the SE yield, while the excess photogenerated electron−hole pairs raise the average electron energy within the illumination region, leading to increased SE yield and a bright contrast regardless of dopant types.[28] This transition will be discussed in more detail in a later section.

2. SPV Signal Dependence on Electron Beam Energy and Laser Fluence. To verify the SPV effect on SE emission, measurements were performed by varying the accelerating voltage. It is known that SEs of electronic origin are generated from the topmost surface region of sample (<10 nm), which is within the width of the SCR caused by the surface band bending in doped semiconductors, and contribute to the SPV contrast. At lower accelerating voltages, the shorter primary electron penetration depths have more overlap with the width of the SCR, so the contribution from the SCR, and thus the SPV effect, have the most contribution to the SE yield change,[16] whereas at higher accelerating voltages, the interaction volume of primary electrons increases, leading to a decrease of the contribution from the surface region. In addition, from eq 7, higher primary electron energies also lead to a lower SE yield to begin with (the primary electron energy for maximum SE yield in silicon is ∼450 eV[20]). As a result, SE emission related with the SPV effect in the doped Si with light illumination is expected to show an electron beam energy dependence.

We plot the optical-fluence-dependent amplitudes of the ETD signal measured with different primary electron energies in Figure 3 (the modulation frequency was fixed at 50 kHz). The plotted data exclude the contribution from the laser leakage through the ETD, while the amplitude scales are calibrated with respect to the laser leakage signal collected with the same experimental conditions. As shown in Figure 3a regarding the measurement of heavily doped n-type Si, the signal amplitude as a function of the optical pump fluence shows an increasing trend toward saturation at 2 keV, indicating the photoinduced band flattening process discussed above. When the accelerating voltage is increased from 2 to 5 and 10 keV, the signal amplitude is much suppressed, which confirms the more significant contribution from the SPV effect at a lower electron beam energy (2 keV) and, in general, a lower SE yield with higher primary electron energies. The p-doped sample (Figure 3b,d) also shows a reduced amplitude and reduced laser fluence dependency at higher electron beam

https://dx.doi.org/10.1021/acs.jpca.0c02543
J. Phys. Chem. A XXXX, XXX, XXX−XXX

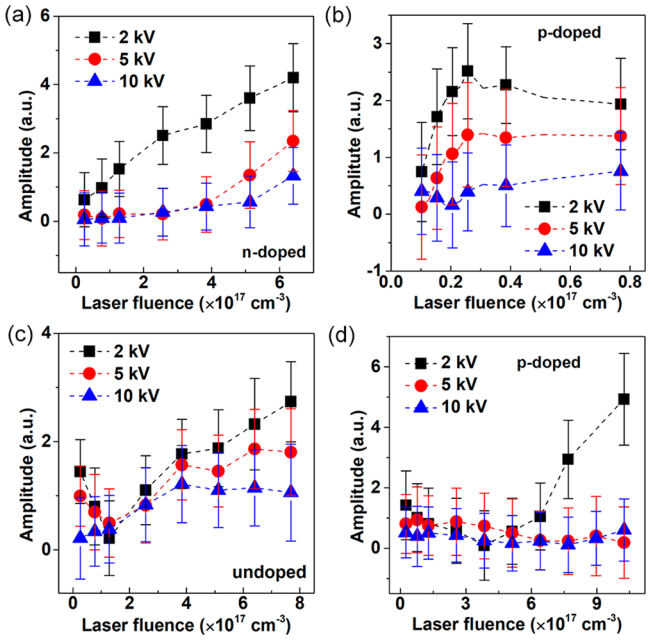

Figure 3. Amplitude signal taken at various electron beam accelerating voltages (2, 5, and 10 keV) for (a) n-doped, (b), (d) p-doped, and (c) undoped Si samples as a function of laser fluence. The modulation frequency for all measurements shown here was 50 kHz. For the doped Si samples, the doping concentration is in the range of 10^{19} cm^{-3}.

voltages. In contrast, for the undoped Si, which has a weak SPV effect, there is a notable signal for all the voltages applied, indicating that the major contribution is caused by the excess electron−hole pairs photogenerated within the optical absorption depth of the bulk sample (the optical absorption depth is 1 μm in Si for 515 nm light, compared to the penetration depth of hundreds of nanometers of 5 and 10 keV primary electrons).

The optical fluence dependence of the amplitude signal is particularly interesting. In n-type Si, the amplitude signal increases monotonously with the optical fluence. When the SPV effect plays a role, this increasing trend is expected. Even after the surface band bending is fully "flattened" by the photogenerated minority carriers, further increasing the optical fluence will keep increasing the amplitude signal, since photoexcitation increases the local electron energy inside the sample, which enhances SE emission in the absence of surface electric fields.[28,29] In p-type Si, the amplitude signal changes with the optical influence in a more complex way. We plot the amplitude signal measured on the same p-type Si sample in Figure 3b,d, each covering a different range of optical fluences. As shown in Figure 3b, the amplitude signal increases first and then decreases when the optical fluence reaches 2.8×10^{16} cm^{-3}. In this regime, the phase signal is near π (Figure 2c), meaning the dark contrast increases, which is consistent with the expected SPV effect (eq 7). Beyond 2.8×10^{16} cm^{-3}, the surface band bending is fully "flattened" by the photogenerated minority carriers, and further increasing the optical fluence starts to increase the SE yield. This is reflected in the decreasing amplitude signal together with a near-π phase signal. It is noted that the optical fluence at the full compensation point (2.8×10^{16} cm^{-3}) gives us an estimation of the surface states density in our p-type Si sample: $\rho_{s,0} = I_{ph}\eta = 2.8 \times 10^{12}$ cm^{-2}, where the optical penetration depth η of 515 nm light is 1 μm in Si. This value is consistent with the typical reported range around 10^{11}−10^{13} cm^{-2}.[24] We can further estimate the SPV at this "flat-band" fluence to be 60 mV using eq 2. From Figure 3d, near an optical fluence of 3.5×10^{17} cm^{-3}, the amplitude signal reaches a minimum near zero, indicating the SE yield at this optical fluence is restored to the intrinsic level without photoexcitation. Above this optical fluence, the phase signal is reversed to be near zero, implying a bright contrast is observed in this regime. This nonmonotonous behavior of the amplitude signal in p-type Si showcases the complex surface photocarrier dynamics in the presence of the SPV effect.

3. SPV Signal Dependence on the Modulation Frequency of the Optical Pump. The modulation frequency dependence of the amplitude signal reflects how fast the system being measured can respond to the modulated photoexcitation. Specifically, if the time constant of the system is τ, the amplitude signal $R(\omega)$ should scale as $R(\omega) = \frac{1}{\sqrt{1+\omega^2\tau^2}}$, where ω is the angular frequency.[30] The amplitude signals of the laser leakage, n-type Si, and p-type Si as a function of the modulation frequency for different optical fluences are shown in Figure 4 (measured at 2 keV primary electron energy). For the laser leakage signal, the time constant τ is the intrinsic response time of our instrument, mainly limited by the response time of the scintillator used in the ETD. From Figure 4a, we extract this time constant to be

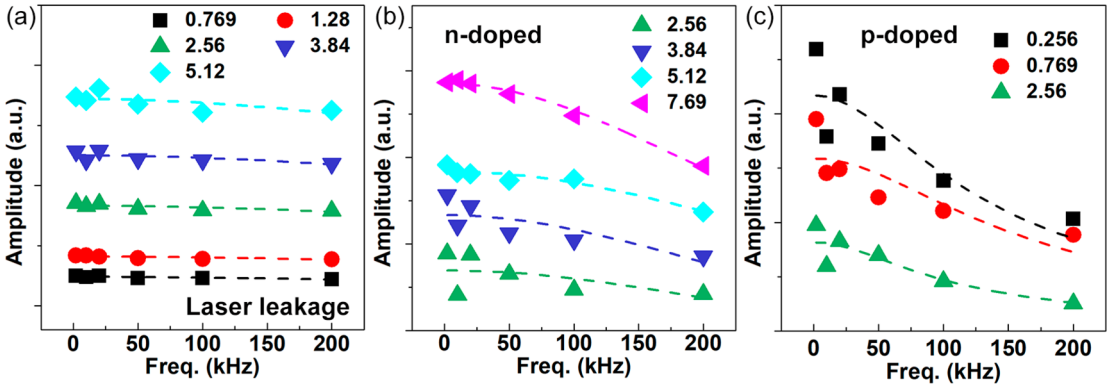

Figure 4. Modulation frequency dependence of the amplitude signal of (a) light leakage into the ETD, (b) n-type Si, and (c) p-type Si with different optical pump fluences (shown in the legend, in unit of 10^{17} cm^{-3}). The doping concentration for the specimens is in the range of 10^{19} cm^{-3}. The primary electron energy used is 2 keV.

https://dx.doi.org/10.1021/acs.jpca.0c02543
J. Phys. Chem. A XXXX, XXX, XXX−XXX

approximately 300 ns, which is consistent with the response time of the scintillating phosphor used in our ETD (P47).[31] For n-type Si and p-type Si, the measured time constant includes both the instrument response and the response time of the sample, which characterizes the time scale of the transport and the surface recombination of the surface photocarriers driven by the built-in electric field. We extract the time constants to be 600 ns for n-type Si and 1.8 μs for p-type Si. The different time constants may indicate a higher surface states density in our n-type Si sample than that of the p-type sample, which is consistent with a faster rise of the amplitude signal in Figure 3b (compared to Figure 3a).

We note here that the working frequencies of our LIA are limited to 500 kHz, which is insufficient to provide more accurate estimation of the time scales of interest. A future upgrade of our experimental apparatus with higher obtainable modulation frequencies can, in principle, generate more accurate estimations of the time scales of the surface photocarrier transport. Nevertheless, the time scales extracted from our current measurements are reasonable compared to literature values. For example, Long et al. used time-resolved photoemission spectroscopy to estimate a SPV relaxation time scale of ~1 μs in silicon.[32] Ogawa et al. used the same technique to measure a time constant of 503 ns of a 300 mV SPV effect in silicon,[33] while Spencer et al. measured a time constant of 6.6 μs of a 440 mV SPV effect in an n-type silicon.[34] Widdra et al. reported a time scale of 800 ns within which the SPV decayed from 300 mV to 100 mV at a SiO_2/Si interface.[35] While the microsecond time scale is consistent among previous time-resolved measurements of the SPV effect, the spread of the time constants indicates the complex dependence of the SPV effect on the sample conditions.

CONCLUSIONS

In summary, we demonstrated a method for determining the SPV effect with the aid of photoassisted SE emission implemented inside a standard SEM coupled with a modulated laser source. In this setup, a pulsed laser generates transient SPV upon superband illumination, and the SE signal is recorded via a LIA. With a low-energy electron beam, the SE yield is strongly influenced by the surface-induced band bending effects. Accordingly, the phase signal can be used to determine the doping type and sample surface conditions. The amplitude signal dependence on the optical fluence and the modulation frequency of the optical beam reveals the complex transport processes of the photocarriers in the presence of a surface electric field. This methodology provides a new way to study the surface photocarrier dynamics, specifically with a nanometer spatial resolution granted by the SEM. We envision that this technique can be particularly promising for characterizing surface photocarrier dynamics of emerging nanostructured materials, including two-dimensional materials, nanoscale junctions and grain boundaries, and nanostructured surfaces. Although the laser beam is relatively large (in principle, the beam diameter can be further reduced to near the diffraction limit by improving the optics), the response from a nanostructured sample can vary locally, which can then be captured using this technique by parking the electron beam at locations of interest. Furthermore, our result provides a basis for quantitative understanding of the contrast mechanisms of emerging time-resolved electron microscopic techniques, such as scanning ultrafast electron microscopy.[29,36]

AUTHOR INFORMATION

Corresponding Author

Bolin Liao − *Department of Mechanical Engineering, University of California, Santa Barbara, California 93110, United States;* orcid.org/0000-0002-0898-0803; Email: bliao@ucsb.edu

Authors

Yu Li − *Department of Mechanical Engineering, University of California, Santa Barbara, California 93110, United States*

Usama Choudhry − *Department of Mechanical Engineering, University of California, Santa Barbara, California 93110, United States*

Jeewan Ranasinghe − *Department of Mechanical Engineering, University of California, Santa Barbara, California 93110, United States*

Alex Ackerman − *Department of Mechanical Engineering, University of California, Santa Barbara, California 93110, United States*

Complete contact information is available at: https://pubs.acs.org/10.1021/acs.jpca.0c02543

Notes

The authors declare no competing financial interest.

ACKNOWLEDGMENTS

This work is partially supported by the US Army Research Office Young Investigator Program under the award number W911NF-19-1-0060 and the National Science Foundation under the award number DMR-1905389 (for the development of the technique) and a Faculty Research Award from the Sony Corporation (for understanding photocarrier dynamics in semiconductors).

REFERENCES

(1) Zangwill, A. *Physics at Surfaces*; Cambridge University Press: New York, 1988.

(2) Zhang, Z.; Yates, J. T. Band Bending in Semiconductors: Chemical and Physical Consequences at Surfaces and Interfaces. *Chem. Rev.* **2012**, *112* (10), 5520−5551.

(3) Najafi, E.; Scarborough, T. D.; Tang, J.; Zewail, A. Four-Dimensional Imaging of Carrier Interface Dynamics in p-n Junctions. *Science* **2015**, *347* (6218), 164−167.

(4) Kronik, L.; Shapira, Y. Surface Photovoltage Phenomena: Theory, Experiment, and Applications. *Surf. Sci. Rep.* **1999**, *37* (1), 1−206.

(5) Chen, R.; Fan, F.; Dittrich, T.; Li, C. Imaging Photogenerated Charge Carriers on Surfaces and Interfaces of Photocatalysts with Surface Photovoltage Microscopy. *Chem. Soc. Rev.* **2018**, *47* (22), 8238−8262.

(6) Wong, E. L.; Winchester, A. J.; Pareek, V.; Madéo, J.; Man, M. K. L.; Dani, K. M. Pulling Apart Photoexcited Electrons by Photo-inducing an In-Plane Surface Electric Field. *Science Advances* **2018**, *4* (9), No. eaat9722.

(7) Najafi, E.; Jafari, A. Ultrafast Imaging of Surface-Exclusive Carrier Dynamics in Silicon. *J. Appl. Phys.* **2019**, *125* (18), 185303.

(8) Demuth, J. E.; Thompson, W. J.; DiNardo, N. J.; Imbihl, R. Photoemission-Based Photovoltage Probe of Semiconductor Surface and Interface Electronic Structure. *Phys. Rev. Lett.* **1986**, *56* (13), 1408−1411.

(9) Cahill, D. G.; Hamers, R. J. Surface Photovoltage of Ag on Si(111)-7 × 7 by Scanning Tunneling Microscopy. *Phys. Rev. B: Condens. Matter Mater. Phys.* **1991**, *44* (3), 1387−1390.

(10) Donchev, V.; Kirilov, K.; Ivanov, Ts.; Germanova, K. Surface Photovoltage Phase Spectroscopy - a Handy Tool for Characterisation

of Bulk Semiconductors and Nanostructures. *Mater. Sci. Eng., B* **2006**, *129* (1), 186−192.
(11) Melitz, W.; Shen, J.; Kummel, A. C.; Lee, S. Kelvin Probe Force Microscopy and Its Application. *Surf. Sci. Rep.* **2011**, *66* (1), 1−27.
(12) Neppl, S.; Shavorskiy, A.; Zegkinoglou, I.; Fraund, M.; Slaughter, D. S.; Troy, T.; Ziemkiewicz, M. P.; Ahmed, M.; Gul, S.; Rude, B.; et al. Capturing Interfacial Photoelectrochemical Dynamics with Picosecond Time-Resolved X-Ray Photoelectron Spectroscopy. *Faraday Discuss.* **2014**, *171* (0), 219−241.
(13) Reshchikov, M. A.; Foussekis, M.; Baski, A. A. Surface Photovoltage in Undoped n-Type GaN. *J. Appl. Phys.* **2010**, *107* (11), 113535.
(14) Yun, J. S.; Seidel, J.; Kim, J.; Soufiani, A. M.; Huang, S.; Lau, J.; Jeon, N. J.; Seok, S. I.; Green, M. A.; Ho-Baillie, A. Critical Role of Grain Boundaries for Ion Migration in Formamidinium and Methylammonium Lead Halide Perovskite Solar Cells. *Adv. Energy Mater.* **2016**, *6* (13), 1600330.
(15) Donchev, V. Surface Photovoltage Spectroscopy of Semiconductor Materials for Optoelectronic Applications. *Mater. Res. Express* **2019**, *6* (10), 103001.
(16) El-Gomati, M.; Zaggout, F.; Jayacody, H.; Tear, S.; Wilson, K. Why Is It Possible to Detect Doped Regions of Semiconductors in Low Voltage SEM: A Review and Update. *Surf. Interface Anal.* **2005**, *37* (11), 901−911.
(17) Chang, T. H. P.; Nixon, W. C. Electron Beam Induced Potential Contrast on Unbiased Planar Transistors. *Solid-State Electron.* **1967**, *10* (7), 701−704.
(18) Perovic, D. D.; Castell, M. R.; Howie, A.; Lavoie, C.; Tiedje, T.; Cole, J. S. W. Field-Emission SEM Imaging of Compositional and Doping Layer Semiconductor Superlattices. *Ultramicroscopy* **1995**, *58* (1), 104−113.
(19) Venables, D.; Jain, H.; Collins, D. C. Secondary Electron Imaging as a Two-Dimensional Dopant Profiling Technique: Review and Update. *J. Vac. Sci. Technol., B: Microelectron. Process. Phenom.* **1998**, *16* (1), 362−366.
(20) Lin, Y.; Joy, D. C. A New Examination of Secondary Electron Yield Data. *Surf. Interface Anal.* **2005**, *37* (11), 895−900.
(21) Flesner, L. D.; O'Brien, M. E. Photovoltage Scanning Electron Microscopy. *Appl. Phys. Lett.* **1989**, *54* (13), 1259−1261.
(22) Sealy, C. P.; Castell, M. R.; Wilshaw, P. R. Mechanism for Secondary Electron Dopant Contrast in the SEM. *J. Electron Microsc.* **2000**, *49* (2), 311−321.
(23) Elliott, S. L.; Broom, R. F.; Humphreys, C. J. Dopant Profiling with the Scanning Electron Microscope—A Study of Si. *J. Appl. Phys.* **2002**, *91* (11), 9116−9122.
(24) Volotsenko, I.; Molotskii, M.; Barkay, Z.; Marczewski, J.; Grabiec, P.; Jaroszewicz, B.; Meshulam, G.; Grunbaum, E.; Rosenwaks, Y. Secondary Electron Doping Contrast: Theory Based on Scanning Electron Microscope and Kelvin Probe Force Microscopy Measurements. *J. Appl. Phys.* **2010**, *107* (1), 014510.
(25) Dionne, G. F. Effects of Secondary Electron Scattering on Secondary Emission Yield Curves. *J. Appl. Phys.* **1973**, *44* (12), 5361−5364.
(26) Kuhr, J.-C.; Fitting, H.-J. Monte Carlo Simulation of Electron Emission from Solids. *J. Electron Spectrosc. Relat. Phenom.* **1999**, *105* (2), 257−273.
(27) Schreiber, E.; Fitting, H.-J. Monte Carlo Simulation of Secondary Electron Emission from the Insulator SiO_2. *J. Electron Spectrosc. Relat. Phenom.* **2002**, *124* (1), 25−37.
(28) Liao, B.; Najafi, E.; Li, H.; Minnich, A. J.; Zewail, A. H. Photo-Excited Hot Carrier Dynamics in Hydrogenated Amorphous Silicon Imaged by 4D Electron Microscopy. *Nat. Nanotechnol.* **2017**, *12* (9), 871.
(29) Liao, B.; Najafi, E. Scanning Ultrafast Electron Microscopy: A Novel Technique to Probe Photocarrier Dynamics with High Spatial and Temporal Resolutions. *Materials Today Physics* **2017**, *2*, 46−53.
(30) Sundaresan, K. R.; Krishnaswamy, P. R. Estimation of Time Delay Time Constant Parameters in Time, Frequency, and Laplace Domains. *Can. J. Chem. Eng.* **1978**, *56* (2), 257−262.
(31) Hoess, P.; Fleder, K. Response of Very-Fast-Decay Phosphors in Image Intensifier Tubes for CCD Readout Devices. In *SPIE Proceedings Vol. 4183, Proceedings of the 24th International Congress on High-Speed Photography and Photonics*, Sendai, Japan, Sept 24−29, 2000; Takayama, K., Saito, T., Kleine, H., Timofeev, E., Eds.; SPIE, 2000.
(32) Long, J. P.; Sadeghi, H. R.; Rife, J. C.; Kabler, M. N. Surface Space-Charge Dynamics and Surface Recombination on Silicon (111) Surfaces Measured with Combined Laser and Synchrotron Radiation. *Phys. Rev. Lett.* **1990**, *64* (10), 1158−1161.
(33) Ogawa, M.; Yamamoto, S.; Kousa, Y.; Nakamura, F.; Yukawa, R.; Fukushima, A.; Harasawa, A.; Kondoh, H.; Tanaka, Y.; Kakizaki, A.; et al. Development of Soft X-Ray Time-Resolved Photoemission Spectroscopy System with a Two-Dimensional Angle-Resolved Time-of-Flight Analyzer at SPring-8 BL07LSU. *Rev. Sci. Instrum.* **2012**, *83* (2), 023109.
(34) Spencer, B. F.; Graham, D. M.; Hardman, S. J. O.; Seddon, E. A.; Cliffe, M. J.; Syres, K. L.; Thomas, A. G.; Stubbs, S. K.; Sirotti, F.; Silly, M. G.; et al. Time-Resolved Surface Photovoltage Measurements at n-Type Photovoltaic Surfaces: Si(111) and ZnO(10$\bar{1}$0). *Phys. Rev. B: Condens. Matter Mater. Phys.* **2013**, *88* (19), 195301.
(35) Widdra, W.; Bröcker, D.; Gießel, T.; Hertel, I. V.; Krüger, W.; Liero, A.; Noack, F.; Petrov, V.; Pop, D.; Schmidt, P. M.; et al. Time-Resolved Core Level Photoemission: Surface Photovoltage Dynamics of the SiO_2/Si(100) Interface. *Surf. Sci.* **2003**, *543* (1), 87−94.
(36) Yang, D.-S.; Liao, B.; Mohammed, O. F. Scanning Ultrafast Electron Microscopy: Four-Dimensional Imaging of Materials Dynamics in Space and Time. *MRS Bull.* **2018**, *43* (7), 491−496.

https://dx.doi.org/10.1021/acs.jpca.0c02543
J. Phys. Chem. A XXXX, XXX, XXX−XXX